Evolution of Electron Phase-Space Holes in a 2D Magnetized Plasma

M. Oppenheim,* D. L. Newman, and M. V. Goldman

Center for Integrated Plasma Studies, University of Colorado, Boulder, Colorado 80309

(Received 12 April 1999)

The nonlinear stage of the two-stream instability in a 2D magnetized plasma produces electron phase-space tubes, the counterpart of phase-space holes in a 1D plasma. These tubes align primarily perpendicular to the magnetic field $\mathbf{B}_0$ and have self-consistent bipolar electric fields parallel to $\mathbf{B}_0$. Such bipolar electric fields have recently been observed in four different regions of the Earth's space plasma environment. Massively parallel 2D kinetic simulations show the dynamics of tube formation, evolution, and breakup, accompanied by the generation of electrostatic whistler waves. We focus on the breakup of the tubes and describe a new numerical study of tube stability.

PACS numbers: 52.35.Qz, 52.35.Sb, 52.65.Rr, 94.20.Rr

It has long been recognized that, in 1D, counterstreaming beams of electrons which intersect generate the two-stream instability and, after saturation, long-lived structures of depleted electron density. These structures appear as rotating vortices of trapped particles around "holes" in phase-space [1,2]. The nonlinear evolution of these holes has been the subject of substantial theoretical and computational investigations, principally in 1D [3–7]. The phase-space structure of these holes has been modeled using stationary Bernstein-Greene-Kruskal modes of the Vlasov equation [8,9] and has been related to nonlinear Landau damping [10,11]. In higher dimensions, electron phase-space hole physics has received recent attention [12–14] in the interpretation of spacecraft data. In this Letter, we use electrostatic, kinetic simulations to explore the nonlinear dynamics of holes in a 2D magnetized plasma.

Studies of phase-space holes have acquired renewed importance because of recent measurements of bipolar electric field pulses—a signature of phase-space holes—made in the Earth's ionosphere, magnetosphere, and foreshock region. In 1994, Matsumoto *et al.* [15] first identified holes as the origin of bipolar electric fields measured by the GEOTAIL satellite in the Earth's magnetotail. In 1998, FAST satellite instruments measured bipolar electric field pulses in the downward current regions of the auroral ionosphere at $\sim$2000 km altitude [16]. These pulses have also been interpreted as signaling the presence of holes [13,14,17]. The FAST observation was quickly followed by reports that the POLAR antennas had measured similar waveforms at altitudes between 2 and 8.5 Earth radii [18]. Most recently, the same characteristic bipolar signature was measured by WIND in the Earth's foreshock region [19].

The earliest multidimensional simulations of the two-stream instability showed that phase-space holes, which remain stable in 1D, quickly dissipate in an unmagnetized 2D or 3D plasma [1]. However, a magnetic field enables holes to persist in higher dimensions [12,13]. The current simulations extend these results and show that holes in (x, v_x) phase-space generalize to tubes in (x, y, v_x) phase-space, aligned mostly perpendicular to $\mathbf{B}_0$. Further, at late times, these simulations show that tubes and their associated bipolar electric fields break up into structures having comparable sizes parallel and perpendicular to $\mathbf{B}_0$. This Letter discusses the evolution of tubes, focusing on the disintegration of elongated tubes and the concurrent development of electrostatic whistler waves. These simulations are performed in a regime where the roles of ion dynamics and electron transport perpendicular to $\mathbf{B}_0$ are negligible.

Our kinetic simulations use a massively parallel electrostatic particle-in-cell (PIC) algorithm which neglects perturbations in the magnetic field [20]. It is capable of modeling either a finite or infinite magnetic field in 1D or 2D. This code applies periodic boundary conditions to model an initial-value problem and uses "quiet-start" algorithms to minimize particle noise. Running the code on supercomputers enables us to employ up to several times 10^8 particles on meshes resolving up to 1024 by 256 points. Our PIC simulation results have been validated, in the case of an infinite magnetic field, through comparisons with a new simulator that evolves the phase-space distribution of density, $f(x, y, v_x)$, by solving the Vlasov equation numerically.

We first consider the full 2D evolution of phase-space tubes and bipolar structures driven in a magnetized plasma by a two-stream instability. Complementary features of such simulations are presented in Refs. [13,14]. Figure 1 shows a number of key phases in the development, evolution, and breakup of phase-space tubes as reflected in the intensity $|\mathbf{E}|^2$ of their self-consistent (i.e., trapping) electric field. This simulation was initiated with two spatially homogeneous, equal temperature Maxwellian distributions of electrons, one having a mean velocity of $v_x = 0$ and the second with $v_x = 5v_{\text{th}}$, where v_{th} is the thermal velocity of each distribution. It also includes a Maxwellian distribution of hydrogen ions with a mean velocity of $v_x = 0$ and a temperature matching that of a single initial electron distribution. The

 0031-9007/99/83(12)/2344(4)$15.00 © 1999 The American Physical Society

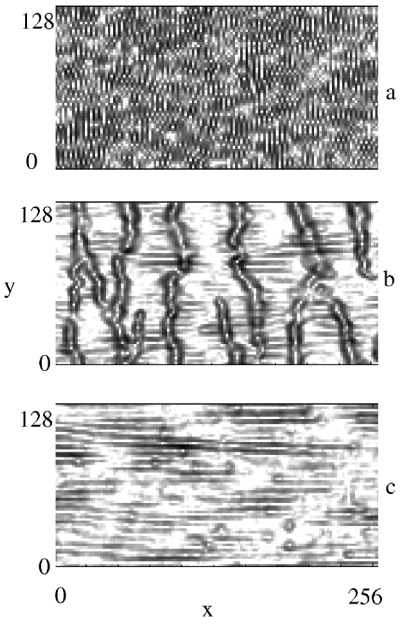

FIG. 1. The three images show electric field energy as a function of $\hat{x}$, parallel to $\mathbf{B}_0$, and $\hat{y}$, perpendicular to $\mathbf{B}_0$, from the 2D PIC simulations at three different times: (a) at $24\omega_e^{-1}$, (b) at $448\omega_e^{-1}$, and (c) at $1920\omega_e^{-1}$. x and y are in units of grid cells where each grid cell spans $\sim$1.5 debye lengths. The darker shades indicate larger values of the log of E^2 with black showing $E^2_{\max}$ and white showing values below $10^{-3}E^2_{\max}$. The images show only the left-hand most quarter of the total simulation box. For animations, see Ref. [22].

magnetic field was chosen so that the ratio of the electron cyclotron frequency to the plasma frequency equals five ($\Omega_e/\omega_e = 5$). The simulation spans 1024 grid points parallel to $\mathbf{B}_0$ ($\hat{x}$ direction) and 128 perpendicular ($\hat{y}$ direction). Each grid point spans roughly 1.5 debye lengths where the debye length is calculated from the late-time, saturated state temperature of all the electrons, which is roughly 2.6 times the temperature of each initial electron distribution.

During the early, linear stage of the two-stream instability, shown in Fig. 1a, one observes a substantial degree of wave coherence develop perpendicular to $\mathbf{B}_0$. This coherence derives from cross $\mathbf{B}_0$ field communication via electric fields, as specified by the Poisson equation, because the magnetic field strongly inhibits cross-field transport of electrons. The coherence develops during the linear growth phase because initially incoherent electron density fluctuations which have the same sign at neighboring y values contribute constructively to E_x, thereby reinforcing one-another's amplification, whereas those having opposite signs contribute destructively. Through this mechanism, the linear instability preferentially creates electron tubes with coherence over a continuous range in y.

After the linear stage (a few plasma frequency periods, ω_e^{-1}), nonlinear kinetic effects develop—primarily particle trapping. At the start of the nonlinear phase, the distribution of electrons trapped in x forms an ensemble of closely packed tubes elongated in y. These tubes interact with one another displaying a rich array of nonlinear dynamical behaviors. The first interaction which becomes apparent is the merging of tubes—a generalization of merging 1D holes [21]. In 2D, because tubes are not perfectly straight, merging typically begins at the point of closest approach between two tubes. The merger then propagates perpendicular to $\mathbf{B}_0$, essentially "zipping" the tubes together. However, sometimes only parts of the tubes merge completely, with the remainder breaking off to form independent tube segments. In this simulation, a large number of tube segments initially form. When two segments with overlapping but not identical extents perpendicular to $\mathbf{B}_0$ merge, a longer tube is produced. A series of such mergings creates tubes hundreds of debye lengths long, as the bipolar field structures show in Fig. 1b. The dynamical processes leading to this stage are clearly visible in the animations of $|\mathbf{E}|$ [22].

Over the next few thousand plasma periods, the bipolar electric fields diminish in amplitude and break into shorter segments—as do the underlying phase-space tubes. By the time corresponding to Fig. 1c, the tubes and field structures have developed comparable scales in x and y. After this point, the qualitative character of the electric fields does not appear to undergo further evolution—at least for the many thousands of ω_e^{-1}.

Simultaneously with the tube breakup, electrostatic whistler waves appear and grow. These whistlers show up as the nearly horizontal streaks in Figs. 1b and 1c. Electrostatic whistlers are a generalization of Langmuir waves in a highly magnetized plasma where the wave vector is oblique to $\mathbf{B}_0$ [23]. They have the fluid dispersion relation in the electron center-of-mass frame $\omega = \omega_e \cos\theta$, where θ is the angle between $\mathbf{k}$ and $\mathbf{B}_0$. This dispersion arises because, in a sufficiently magnetized plasma, electrons respond only to the parallel component of the electric field, $E_x = E\cos\theta$. The primary whistler waves that develop in the simulations have a θ near 90°, making them low frequency waves. The small k_x of these whistlers necessitates the large simulation size parallel to $\mathbf{B}_0$ employed here.

In order to better understand the breakup of phase-space tubes, we performed a simulation which numerically analyzes the stability of 1D tubes in 2D. This simulation was run without dynamic ions and with infinite magnetization. The validity of assuming an infinite magnetic field was tested by showing that full two-stream simulations with $\Omega_e/\omega_e = 5$ and $\Omega_e \to \infty$ yield virtually identical results. A similar comparison showed that H^+ ions also had little effect on the evolution of phase-space tubes.

This new simulation was initiated with the same counterstreaming electron beams as above, except with $E_x(x, y)$ replaced by the y-averaged electric field, $\overline{E_x}(x) = 1/l \int_0^l E_x(x, y)\, dy$, effectively making this a 1D simulation. After many thousand ω_e^{-1}, this simulation

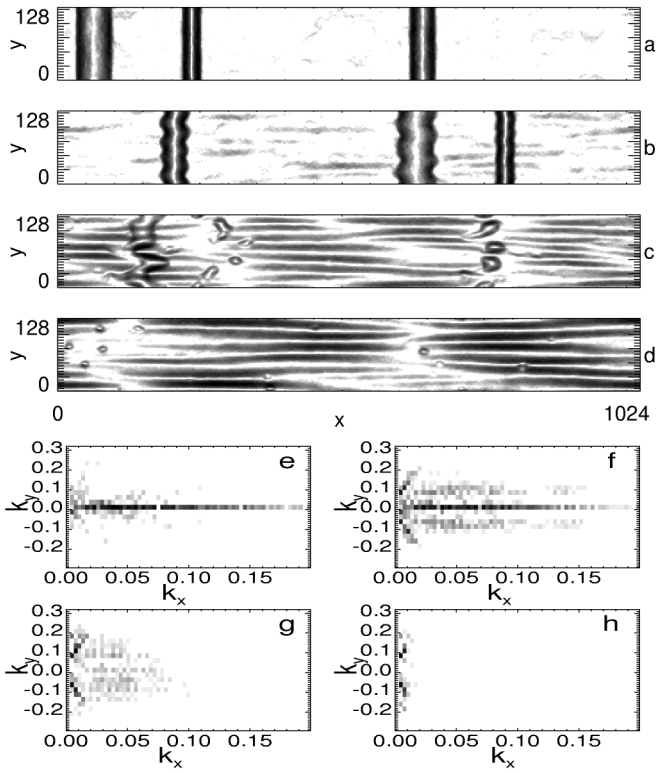

FIG. 2. Electric field energy plotted versus $\hat{x}$ and $\hat{y}$ from a 2D simulation initialized with three stable 1D tubes at four different times: (a) at 0, (b) at $320\omega_e^{-1}$, (c) at $640\omega_e^{-1}$, and (d) at $1760\omega_e^{-1}$. The shading has the same meaning as in Fig. 1, but, now, x and y are in units of grid cells where each grid cell spans $\sim$0.75 debye lengths. Images (e)–(h) show $|\mathbf{E}(k_x, k_y)|$ at these same times and show the migration of energy from tubes to whistlers.

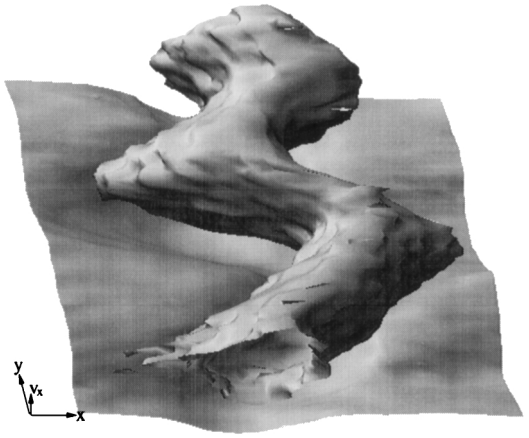

FIG. 3. Isosurface of phase-space tube taken from a two-stream simulation without ions. This image shows an isosurface of a single value of phase-space, $f(x, y, v_x) = c$, averaged over v_y. The tube results from the reduced electron density inside the 2D electron phase-space hole. The sheet below the tube results from passing particles. An upper sheet of passing particles traveling in the opposite direction as the lower sheet particles have been removed to show the tube.

stabilized into three 1D tubes as shown in Fig. 2a. At this point the electric fields were made fully 2D. The subsequent evolution reveals that the straight structures are unstable, developing kinks as seen in Figs. 2b and 2c. The kinks grow in amplitude until the structures break up, as in the full 2D simulation of Fig. 1, and evolve into the long-lived state shown in Fig. 2d. Simultaneously with the kinking of the tubes, electrostatic whistler waves develop and grow as seen in Figs. 2b–2d. Figure 3 shows a snapshot of a tube in (x, y, v_x) phase-space, as characterized by an isosurface of f_e, during the stage of kinking and whistler wave growth from a two-stream simulation.

Figures 2e–2h show the **k**-space spectral distribution of wave amplitude $|\mathbf{E}_k|$ at the same four times as the real-space plots (Figs. 2a–2d). The intense modes at $k_y = 0$ in Fig. 2e arise from the spectrum of the 1D tubes. At time $320\omega_e^{-1}$, the real-space kinks (Fig. 2b) appear as vertically displaced sidebands in **k** space (Fig. 2f). The whistlers appear simultaneously in the spectrum as the intense modes with the same k_y as the kink sidebands except $k_x \ll k_y$. Thus we can conclude that the whistlers and kinks have the same vertical wave number (note, that the apparent whistler wavelength in the real-space plots is half the true wavelength because we are plotting $|\mathbf{E}|$). Also, the kinks oscillate with the same frequency as the whistlers when viewed from the frame of the tubes. The dynamical behavior appears clearly in the animations [22].

As the system continues to evolve, the tubes break into pieces with perpendicular sizes comparable to the vertical wavelength of the electrostatic whistler waves (Fig. 2c). This breakup is associated with a broadening in the sideband spectra (Fig. 2g). After a few thousand additional plasma periods, the distribution of electric fields in this 1D $\Rightarrow$ 2D simulation (Fig. 2d) appears similar to those in the full 2D simulation of Fig. 1c. At this point, the whistlers contain the bulk of the wave energy, as seen in the **k** spectrum (Fig. 2h).

Although the details of how the kinking phase-space tubes interact with the whistlers remains unclear, we can nevertheless monitor the intensity of $|E_y|$, which is dominated by the whistlers, as a measure of the rate of whistler growth. Figure 4 shows the spatial average of $\langle|E_y|\rangle$. The approximately straight portion of the curve suggests a period of exponential growth, which may be associated with a linear instability. However, since this segment spans only $\sim$1 order of magnitude in wave intensity, further confirmation is needed.

In addition to the simulations discussed above, we have performed related simulations with a wide variety of parameters. We comment on these other runs here only insofar as they impact on the evolution of electron phase-space tubes.

In 1D simulations, properties of the ion distribution (e.g., mass, mean velocity, and temperature) affect the

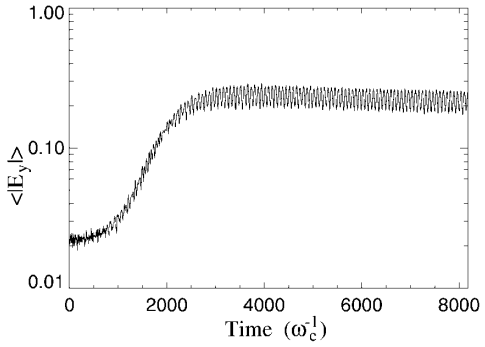

FIG. 4. The spatially averaged perpendicular electric field squared ($\sqrt{\langle E_y^2 \rangle}$) shows the growth of whistler waves in the 1D $\Rightarrow$ 2D simulations.

formation and evolution of electron phase-space holes [7]. However, for the simulation of Fig. 1, the H^+ ions have little measurable effect on the tubes even though the same ion distribution in an otherwise equivalent 1D simulation causes electron phase-space holes to deteriorate over a period of several thousand ω_e^{-1}. Depending on the properties of the ion distribution, ions may significantly impact the 2D dynamics, as evidenced by the presence of lower hybrid waves in these simulations [14].

The formation, evolution, and breakup of tubes remains remarkably independent of magnetization level provided $\Omega_e > \omega_e$. By contrast, when $\Omega_e < \omega_e$, the dynamics change dramatically. At the extreme, when $\Omega_e = 0$ (i.e., $\mathbf{B}_0 = 0$), phase-space holes and tubes do not form [1], presumably because electron transport perpendicular to the beam direction destroys them before they have a chance to form. As Ω_e increases from zero toward ω_e, tubes do form. However, their subsequent evolution and decay is different than when $\omega_e < \Omega_e$. Specifically, the tubes are comparatively short lived, and kinks and electrostatic whistler waves do not appear. The lack of whistler waves presumably results from the difference in the linear dispersion relation in these two regimes. When $\Omega_e > \omega_e$, the Langmuir wave branch connects to the electrostatic whistler branch for waves oriented oblique to $\mathbf{B}_0$, whereas, when $\Omega_e < \omega_e$, the Langmuir branch connects to the upper hybrid branch.

Finally, we wish to comment on the circular structures with ringlike maxima in $|\mathbf{E}|^2$, often found after many thousand ω_e^{-1} in the magnetized 2D simulation (cf. Figs. 1c and 2d). A spacecraft antenna measuring electric fields, while passing through one of these structures, would typically detect a bipolar spike parallel to the direction of motion and a comparable unipolar spike in the perpendicular direction, in accord with FAST spacecraft observations [16]. However, in the periodic simulations, the electric field of whistler waves generally dominates E_y. We conjecture that in space the large whistler group velocity parallel to $\mathbf{B}_0$ might advect these waves away from the regions containing the ringlike structures. These structures would then comprise the dominant observable fields.

We would like to thank R. Ergun, L. Muschietti, and S. Parker for a number of useful and informative discussions. The calculations shown here were performed using the computers at the ACL of LANL. This research was supported by funding from NASA and NSF.

*Present address: Astronomy Department, Boston University, Boston, MA 02215.

[1] R. L. Morse and C. W. Nielson, Phys. Rev. Lett. **23**, 1087 (1969).
[2] H. L. Berk, C. E. Nielson, and K. V. Roberts, Phys. Fluids **13**, 980 (1970).
[3] R. L. Morse and C. W. Nielson, Phys. Fluids **12**, 2418 (1969).
[4] T. H. Dupree, Phys. Fluids **25**, 277 (1982).
[5] V. A. Turikov, Phys. Scr. **30**, 73 (1984).
[6] J. P. Lynov *et al.*, Phys. Scr. **31**, 596 (1985).
[7] Y. Omura, H. Matsumoto, T. Miyake, and H. Kojima, J. Geophys. Res. **101**, 2685 (1996).
[8] I. B. Bernstein, J. M. Greene, and M. D. Kruskal, Phys. Rev. **108**, 546 (1957).
[9] V. L. Krasovsky, H. Matsumoto, and Y. Omura, J. Geophys. Res. **102**, 22 131 (1997).
[10] M. B. Isichenko, Phys. Rev. Lett. **78**, 2369 (1997).
[11] G. Manfredi, Phys. Rev. Lett. **79**, 2815 (1997).
[12] T. Miyake, Y. Omura, H. Matsumoto, and H. Kojima, J. Geophys. Res. **103**, 11 841 (1998).
[13] M. V. Goldman, M. M. Oppenheim, and D. L. Newman, in *Physics of Space Plasmas*, edited by T. Chang and J. R. Jasperse (MIT Center for Theoretical Geo/Cosmo Plasma Physics, Cambridge, MA, 1998), Vol. 15, pp. 115–120.
[14] M. V. Goldman, M. M. Oppenheim, and D. L. Newman, Geophys. Res. Lett. **26**, 1821 (1999).
[15] H. Matsumoto *et al.*, Geophys. Res. Lett. **21**, 2915 (1994).
[16] R. E. Ergun *et al.*, Geophys. Res. Lett. **25**, 1 (1998).
[17] R. E. Ergun *et al.*, Phys. Rev. Lett. **81**, 826 (1998).
[18] J. R. Franz, P. M. Kintner, and J. S. Pickett, Geophys. Res. Lett. **25**, 1277 (1998).
[19] S. D. Bale *et al.*, Geophys. Res. Lett. **25**, 2929 (1998).
[20] C. K. Birdsall and A. B. Langdon, *Plasma Physics Via Computer Simulation* (McGraw-Hill, New York, 1985).
[21] K. Saeki, P. Michelsen, H. L. Pecseli, and J. J. Rasmussen, Phys. Rev. Lett. **42**, 501 (1979).
[22] See AIP Document No. EPAPS: E-PRLTAO-83-019938 for animations of the evolution of electron phase-space holes in 2D. This document may be retrieved via the EPAPS homepage (http://www.aip.org/pubservs/epaps.html) or from ftp.aip.org in the directory /epaps/. See the EPAPS homepage for more information. An alternate repository is at http://astro.bu.edu/~meerso/EH-movies.
[23] Y. L. Zhang, H. Matsumoto, and Y. Omura, J. Geophys. Res. **98**, 21 353 (1993).